Electron transfer properties of organic dye-sensitized solar cells based on indoline sensitizers with ZnO nanoparticles

2010 Nanotechnology 21 485202

(http://iopscience.iop.org/0957-4484/21/48/485202)

Nanotechnology **21** (2010) 485202 (8pp) doi:10.1088/0957-4484/21/48/485202

Electron transfer properties of organic dye-sensitized solar cells based on indoline sensitizers with ZnO nanoparticles

Hsin-Ming Cheng[1,2,4] **and Wen-Feng Hsieh**[1,3,4]

[1] Department of Photonics and Institute of Electro-Optical Engineering, National Chiao Tung University, Hsinchu 300, Taiwan
[2] Material and Chemical Research Laboratories, Industrial Technology Research Institute, Hsinchu 310, Taiwan
[3] Institute of Electro-Optical Science and Engineering, National Cheng Kung University, Tainan 701, Taiwan

E-mail: SMCheng@itri.org.tw and wfhsieh@mail.nctu.edu.tw

Received 2 August 2010, in final form 14 October 2010
Published 4 November 2010
Online at stacks.iop.org/Nano/21/485202

Abstract
Two indoline dyes, coded D149 and D205, were used as the sensitizers of ZnO dye-sensitized solar cells (DSCs) with optimal energy conversion efficiencies of more than 5%, under AM 1.5 full sunlight illumination (100 mW cm^{-2}). Higher interfacial charge transfer rate and retardant fluorescence decay confirmed from transient fluorescence illustrated that D205-sensitized ZnO DSCs could possess better electron transport than D149-sensitized ZnO DSCs. The enhancement of V_{oc} and J_{sc} for D205-sensitized ZnO DSCs was ascribed to the effective suppression of electron recombination by extending the alkyl chain on the terminal rhodanine moiety from ethyl to octyl. The evidence of enhanced electron diffusion coefficient was further shown by electrochemical impedance spectroscopy (EIS).

(Some figures in this article are in colour only in the electronic version)

1. Introduction

Dye-sensitized solar cells (DSCs) have been expected to be one of the most promising environmental-friendly photovoltaic devices, since they possess the advantages of being flexible, low cost, and easier to manufacture than other brittle thin film solar cells [1, 2]. Designing a sensitizer with a high absorption coefficient in visible even near-IR light is one of the crucial issues. Furthermore, the highest occupied molecular orbital (HOMO) and lowest unoccupied molecular orbital (LUMO) potentials for the designed sensitizers must match with the potential of the redox couple and the conduction band of the photoelectrode, respectively. Numerous metal-free organic dyes with high absorption coefficients have recently been reported to act as good sensitizers for TiO_2. Ruthenium complex dyes are not suitable for environmentally friendly photovoltaic devices because they do not meet the low cost and mass production requirements needed for potentially wide applications. In particular, indoline dyes have been reported to show the highest power conversion efficiency of over 9.0% using volatile electrolytes [3, 4] and efficiency of 7.2% using nonvolatile ionic-liquid electrolytes [5] among organic dyes. Indoline dyes exhibit not only remarkable DSC performance but relatively inexpensive manufacturability due to the simple preparation procedures [6, 7].

As a versatile semiconductor, ZnO has recently been reported as an alternative for DSCs because ZnO offers a large direct band gap of 3.37 eV (similar to TiO_2) and very high electron mobility for its relatively small electron effective mass as compared to TiO_2 [8–10]. ZnO also can be tailored to various architectures, such as nanorods/nanowires [11–15], nanotubes [16, 17], nanoflowers [18], nanosheets [19, 20], tetrapod-like nanopowders [21–23], and polydispersive aggregates [24, 25], which can significantly enhance DSC performance through offering either a large surface area for dye adsorption or direct transport pathways for photo-excited electrons. Besides being employed in TiO_2 photoelectrodes, an indoline dye (coded D149) has recently been utilized with

[4] Authors to whom any correspondence should be addressed.

ZnO nanosheets [20] and tetrapod-like ZnO nanopowders [22] to achieve performances of 4.2% and 4.9%, respectively.

Accordingly, a systematic study of the characterization in indoline-sensitized DSCs is important for both further dye molecular engineering and photovoltaic application points of view. The aim of this paper is to investigate the influence of electron transport on DSCs composed of metal-free organic dyes and hierarchical ZnO photoelectrodes. Two indoline dyes, coded D149 and D205, were clarified as the effective sensitizers for ZnO DSCs. The maximum energy conversion efficiencies of 4.95% and 5.34% were achieved on 27 μm-thick ZnO photoelectrode film under AM 1.5 solar radiation for D149 and D205, respectively. Transient fluorescence and electrochemical impedance spectroscopy (EIS) will also be used to examine the electron transport property of ZnO photoelectrodes with these two indoline dyes.

2. Experiments

2.1. Preparation of ZnO colloidals and screen-printing pastes

The ZnO colloidal solution was produced from zinc acetate dihydrate (99.5% $Zn(OAc)_2$, Riedel–deHaen) in diethylene glycol (99% DEG, TEDIA), similar to what we presented exhaustively before [26, 27]. The as-synthesized solution was placed in a centrifuge operating at 8000 rpm for 30 min. After centrifugation, the precipitation of ZnO colloids was then redispersed in ethanol via high-speed stirring for 30 min. The excess DEG solvent was then removed by a second centrifugation. The ZnO paste for screen-printing was prepared typically by mixing resultant ZnO colloids, ethyl cellulose (EC) and terpineol (anhydrous, #86480, Fluka), the detailed procedure is as follows. EC 5–15 mPa s and EC 30–70 mPa s (#46070 and #46080, Fluka) were individually dissolved in ethanol to yield 10 wt% solution. Then 12 g EC 5–15 and 12 g EC 30–70 were added to a round bottomed rotavap flask containing 12 g ZnO colloids and 25 g terpineol. The mixture paste was dispersed in an ultrasonic bath and a rotary-evaporator (BUCHI V850) was used to remove the residual ethanol and water in the mixture. The final formulations of the ZnO pastes were made with a three-roll mill (EXAKT E50).

2.2. Cell fabrication and characterization

The DSCs were basically sandwiched together with many parts. The photoanodes were prepared by screen-printing the 0.28 cm^2 ZnO films with various thicknesses (18, 21, 27 and 32 μm) on fluorine-doped tin oxide (FTO) substrates (Nippon Sheet Glass Co. Ltd, 10 Ω/square, 3 mm thickness). The photoelectrodes were then gradually heated under an O_2 flow at 350 °C for 30 min to remove the organic materials in the paste. After cooling to room temperature, the ZnO photoelectrodes were immersed into a solution made of 0.3 mM D149 or D205 organic sensitizer (Chemicrea Inc.) with 0.6 mM chenodeoxycholic acid (CDCA, Sigma-Aldrich) in acetonitrile/tert-butyl alcohol mixture (v/v = 1:1) at 65 °C for 1 h. The counter electrodes were also made of NSG FTO glass on which the nanocrystalline Pt catalysts were deposited by decomposing from H_2PtCl_6 at 400 °C for 20 min. The internal space of the ZnO photoelectrodes and counter electrodes was separated by a 60 μm thick hot-melting spacer (Surlyn, DuPont) and filled through a hole with volatile electrolytes, which are composed of 0.5 M 1,2-dimethyl-3-propylimidazolium iodide (PMII), 0.03 M I_2 (Sigma-Aldrich), and 0.5 M tert-butylpyridine (TBP, Sigma-Aldrich) in acetonitrile.

2.3. Instrumentation

The morphology and dimension of ZnO nanoparticles were characterized using a JEOL-6500 field emission scanning electron microscope (FESEM) operated at 5 kV. The advanced ZnO nanostructures were analyzed using a JEOL JEM-2100F field emission transmission electron microscope (FETEM) operated at 200 kV. Optical absorbance was carried out by a Hitachi U-2800 UV–vis spectrophotometer with a tungsten halogen lamp. The steady-state and time-resolved photoluminescence (PL) spectroscopies were monitored using a Jobin-Yvon Triax-320 monochromator with a charge-coupled device and a time-correlated single photon counting (TCSPC) system (PicoHarp 300, PicoQuant), respectively. The pumping apparatus was employed by a frequency-doubled mode-locked Ti:sapphire laser (Mai Tai, Spectra-Physics) to generate output pulses at 400 nm with duration ~100 fs and a repetition rate of 80 MHz. For photocurrent–voltage (J–V) characteristics and electrochemical impedance spectroscopy (EIS) measurements, a white light source (Yamashita Denso, YSS-100A) was used to give an irradiance of 100 mW cm^{-2} equivalent to one sun at AM 1.5 on the surface of the solar cells, and the data were collected by an electrochemical analyzer (Autolab, PGSTAT30). The light power was calibrated with a set of neutral density filters and detected by a silicon photodiode (BS-520, Bunko Keiki). The action spectra of the incident monochromatic photon to current conversion efficiency (IPCE) for solar cells were measured as a function of wavelength from 400 to 900 nm using a specially designed IPCE system (C-995, PV-measurement Inc.) for DSCs.

3. Results and discussion

Hierarchically-packed ZnO nanoparticles were formed in the condensation reactions of the sol–gel process modified from the previous reports [28]. The spherical shape of the secondary ZnO nanoparticles, with diameters in the range of 160–580 nm, is recognized with agglomeration of many primary single crystallites ranging from 6 to 12 nm, as shown in figures 1(a) and (b). The similar ZnO architectures have been elucidated as the random lasers in which the cavities were formed by multiple scattering between ZnO primary particles [29]. The laser action emerges from efficient amplification along the closed loop light-scattering paths within a secondary ZnO nanoparticle. Recently, Cao *et al* have demonstrated that the aggregation of ZnO nanocrystallites performs an effective scheme to generate light scattering within the photoelectrode film of DSCs without using any other scattering layers [24, 25]. In addition, dye-molecule adsorption could be retained

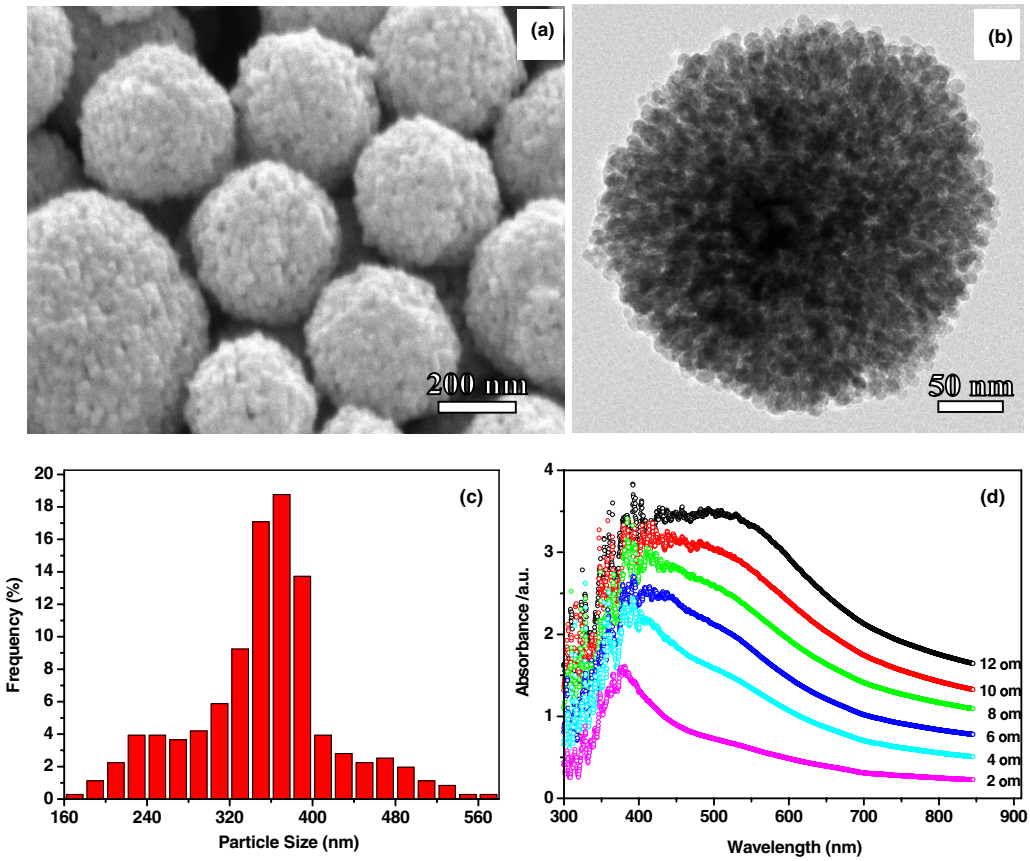

Figure 1. (a) and (b) The FESEM and TEM images for the self-assembled ZnO secondary nanoparticles, respectively. (c) Diameter distribution for the ZnO secondary nanoparticles. (d) The corresponding optical absorption spectra of ZnO photoelectrodes with various film thicknesses, from 2 to 12 μm.

sufficiently due to enough internal surface area provided by the primary nanocrystallites. The maximum energy conversion efficiency of 5.4% has been achieved by utilization of the ruthenium complex *cis*-[$RuL_2(NCS)_2$] (L = 4,4′-dicarboxy-2,2′-bipyridine), N3 dye. Herein, the broad size distribution of secondary nanoparticles with mean radius of 360 nm, as shown in figure 1(c), is controlled to provide the wide range absorption of visible sun light within the preferable packing of the ZnO photoelectrode. The hierarchical ZnO photoelectrode provides the multiple scattering of light and therefore the light-traveling distance can be significantly prolonged. Figure 1(d) also shows the corresponding optical absorption spectra of ZnO photoelectrodes with various film thicknesses. The absorption peak at 375 nm, which could be particularly identified from 2 μm film, mainly resulted from the intrinsic exciton absorption of ZnO. However, the absorption at wavelengths around 400–650 nm is enhanced dramatically by increasing the thickness of the ZnO photoelectrodes from 2 to 12 μm. The ZnO films with thicknesses above 10 μm provide light localization through significant light scattering from the highly disordered structure. The results manifest the light-scattering capability of the films with different thicknesses and the formation of optical confinement through the aggregated ZnO films that could provide more photon absorption in the visible region by the dye molecules.

The double rhodanic acid was used as an anchor moiety for both D149 and D205 sensitizers. The D205 is designed by introducing an octyl substitute onto the terminal rhodanine ring to replace the ethyl group of D149. The detailed molecular structures of the indoline-based organic dyes employed in this study have been depicted in previous reports [4, 5]. Figure 2(a) shows the light absorption spectra and PL spectra of D149 and D205 in acetonitrile at the concentration of 0.015 mM, respectively. The solutions were filled within cuvette cells to avoid thickness and geometry effects. The absorption spectra of D149 and D205 in solution consist of two branches. The 388 nm peak is ascribed to a mixture of intramolecular charge transfer (ICT) and the π–π^* excitation from the HOMO to the LUMO + 1, on the other hand, the main absorption peak, located at 530 nm, is ascribed to an ICT transition from the HOMO to the LUMO [30, 31]. Both the absorption spectra are almost identical, revealing that the D205 dye has almost the same molecular coefficient value of 68 700 M^{-1} cm^{-1} as D149 [7]. The PL spectra of D149 and D205 in solution are also identical with broad peaks at around 660 nm which could be attributed to radiative relaxation. The transition predominantly results from the absorption maximum since the wavelength of excitation is 400 nm. Figure 2(b) shows the light absorption and PL spectra of D149 and D205 on 4 μm-thick ZnO photoelectrodes, respectively. The dye-sensitized ZnO films were prepared by the standard procedure as mentioned in section 2 but covered with pure acetonitrile without the additive redox couple. The absorption spectra of D149 and

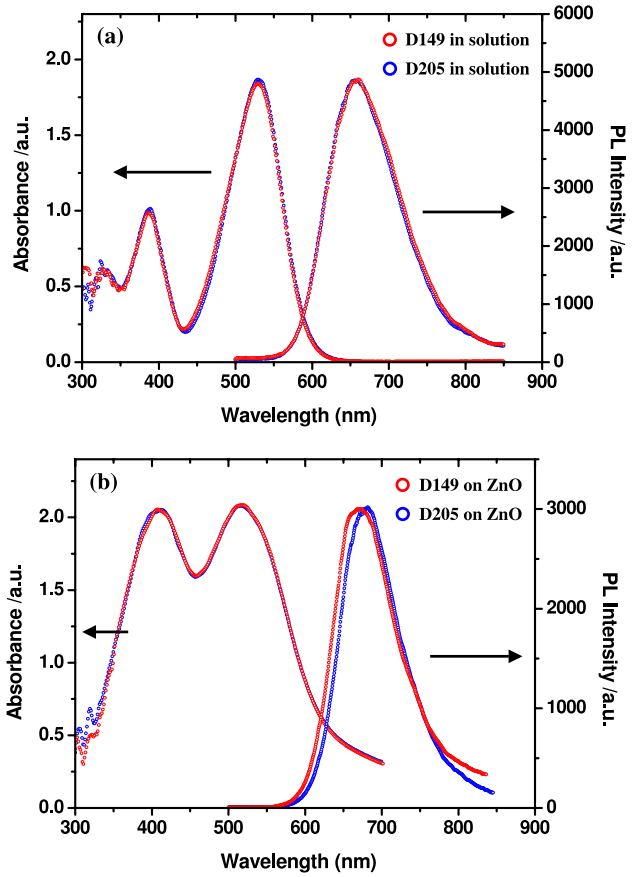

Figure 2. Absorption and photoluminescence spectra of: (a) D149 and D205 dyes in tert-butyl alcohol/acetonitrile (1/1) solution and (b) D149 and D205 dyes anchored on the 4 μm-thick ZnO photoelectrodes.

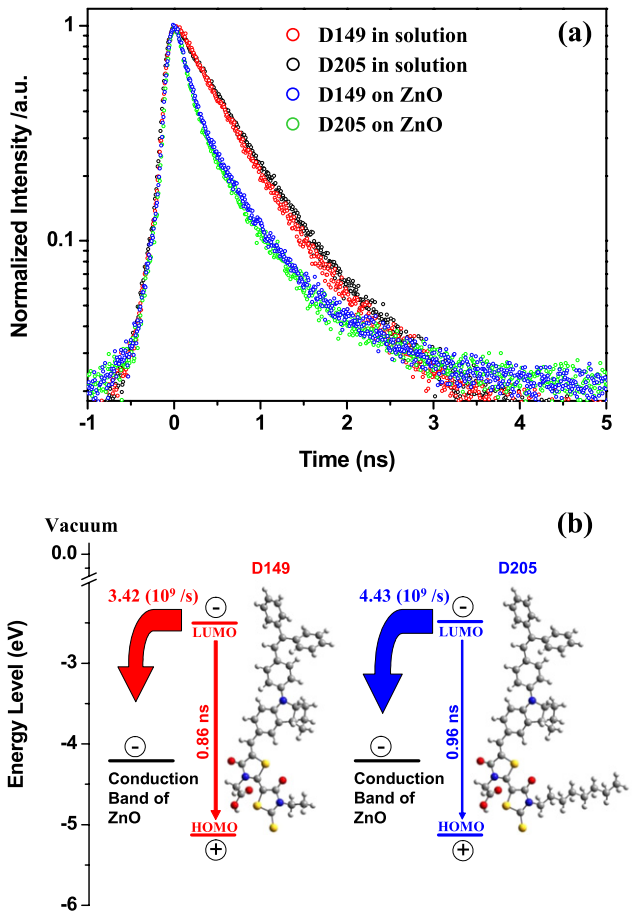

Figure 3. (a) Photoluminescence decay of D149 and D205 dyes in tert-butyl alcohol/acetonitrile (1/1) solution and on ZnO photoelectrodes, respectively. (b) Schematic representation of the charge transfer of photo-excited indoline dyes anchored onto ZnO surfaces. The energy levels of D149 and D205 are sourced from [31]. The vacuum level is defined at 0 eV.

D205 on ZnO photoelectrodes have broadened peaks and blue-shifted main absorption peaks centered around 516 nm, which indicates that these indoline dyes have a moderate interaction between dye molecules on the ZnO surface. The red-shift absorption peaks at low wavelength for indoline dyes on ZnO could be related to the influence of the thickness effect on the photoelectrode. The blue shift of the main absorption peak from 530 nm (indoline dyes in the solution) to 516 nm (indoline dyes on ZnO films) could be addressed as a hypsochromic shift due to plane-to-plane arrangement (H-aggregation). The observation is similar to the previous reports concerning indoline dye on TiO_2 [32]. The origin is mainly attributed to the formation of a bidentate complex between the carboxylate and the polar ZnO surface [33]. Meanwhile the yield of the fluorescence decreases substantially for D149 and D205 on ZnO with respect to D149 and D205 in solution, suggesting the occurrence of PL quenching. Furthermore, the PL spectra consistently move toward a lower energy with respect to those of indoline dye in solution. The observed red-shift in PL spectra indicates that the interface between adsorbed dye molecules and ZnO is strongly bonded which provides effective electron transfer between dye molecules and ZnO. Meanwhile, the polar ZnO surface enhances the delocalization of the π-electrons and lowers the band gap energy of indoline dye. To the 20 nm (from 660 to 680 nm) red-shift for D205 and 10 nm (from 660 to 670 nm) for D149, we presumably ascribe a remarkable bonding force while D205 anchors onto the ZnO surface. However, further investigations on the interactions of dye aggregation are needed for better understanding the dynamics of DSCs.

To investigate the interfacial electron transfer between indoline dye and ZnO, TCSPC studies were employed to provide further information on the electron injection dynamics. Time-dependent fluorescence was collected at the confirmed emission maximum for each specimen from figure 2. Figure 3(a) shows the emission decay recorded with indoline dyes. A biexponential decay kinetics was found to be satisfactory in determination of emission lifetimes. Normally, the PL decay has a fast decay to begin with followed by a slow decay. The fast decay normally results from nonradiative energy transfer or charge transfer with shorter decay time τ_{NR}, while the slow decay is attributed to radiative recombination with longer decay time τ_R. The lifetimes and corresponding amplitudes are listed in table 1. The radiative decay times for pure D149 and D205 in solution are 0.86 and 0.96 ns, respectively. It is apparent that increasing the alkyl chain length results in slower fluorescence decay, indicative of the

Table 1. Kinetic parameters of the indoline dye emission decay analysis. (Note: time coefficients, including lifetime and corresponding amplitude, can be obtained from fitting the biphasic decay. The charge transfer rate constant was estimated from formula (1).)

Indoline dye		a_{NR}	τ_{NR} (ns)	a_R	τ_R (ns)	K_{et} (10^9 s^{-1})
D149	In solution	2641	0.47	1218	0.86	—
D205	In solution	2823	0.55	953	0.96	—
D149	On ZnO	2298	0.18	1524	0.73	3.42
D205	On ZnO	1845	0.16	1192	0.70	4.43

slower radiative recombination. The reduction in the radiative decay times to 0.73 and 0.7 ns for D149 and D205 on ZnO suggests PL quenching as mentioned previously from the decreasing fluorescence yields that appear more dramatically for the D205 dye.

Besides, it should be noted that the dynamics of excited state decay is strongly enhanced for the indoline dyes anchoring onto ZnO surfaces, indicative of a faster interfacial electron transfer behaving as a new relaxation process. The nonradiative decay takes 0.47 and 0.55 ns for D149 and D205 in solution, respectively. However, the nonradiative decay times have dramatically decreased to 0.18 and 0.16 ns for D149 and D205 anchored on ZnO. As a dilute system (indoline dyes in acetonitrile solution) with the concentration of 0.015 mM, the probabilities of intermolecular charge transfer and intermolecular energy transfer are presumably negligible. The nonradiative decay of dyes in solution with $\tau_{NR(Dye)}$ is mainly attributed to intramolecular energy transfer, the observed decrease in nonradiative time $\tau_{NR(Dye+ZnO)}$ for dyes on ZnO is contributed by the additional pathway of charge transfer between the excited state dye and the ZnO surface. Therefore, the charge transfer rate can be evaluated from the nonradiative part by the expression

$$K_{et} = \frac{1}{\tau_{NR(Dye+ZnO)}} - \frac{1}{\tau_{NR(Dye)}}. \quad (1)$$

Here we assume that $\tau_{NR(Dye+ZnO)}$ counts for both energy transfer and charge transfer but $\tau_{NR(Dye)}$ for energy transfer only. The electron transfer rates of 3.42×10^9 and 4.43×10^9 s^{-1} for D149 and D205 on ZnO surfaces are obtained, respectively. We thus conclude that the D205 exhibits efficient electron injection dynamics for ZnO nanoparticles with respect to D149 as a result of faster interfacial electron transfer and retarded fluorescence decay. A simplified diagram describing the mechanism of charge transfer between the indoline dyes and the ZnO interfaces is also presented schematically as figure 3(b).

Figure 4 displays the incident monochromatic photon to current conversion efficiency (IPCE) spectra of DSCs constructed using two indoline dyes with different ZnO photoelectrode thicknesses. Because of the UV cut-off effect caused by the thick glass substrate the spectra at wavelengths shorter than 400 nm are deteriorated. The photocurrent peak at approximately 367 nm is due to direct light harvesting by the ZnO semiconductor which remains almost unchanged while increasing the photoelectrode thickness from 18 to 32 μm because of the short penetration depth for UV light. However, with increase in thickness of the ZnO photoelectrode, the maximal IPCE increases from 71% to 74%

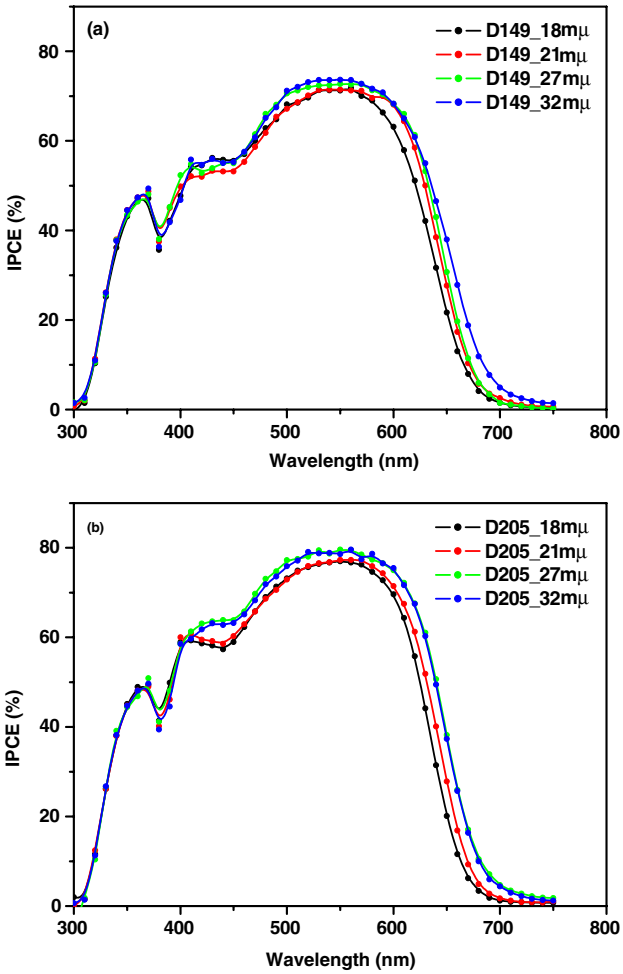

Figure 4. Photocurrent action spectra of ZnO DSCs constructed using (a) D149 and (b) D205, with different photoelectrode thicknesses.

and 77% to 79% at 550 nm for D149- and D205-sensitized ZnO DSCs, respectively. Moreover, the values of IPCE increase significantly in the longer wavelength region (580–700 nm) with thicker photoelectrode films but are saturated at thicknesses above 30 μm because of the limitation of the electron diffusion length. Numerous cracks in thick photoelectrode films (>32 μm) were also observed as a result of unpracticed-printing technology. The optimal IPCE obtained for the D205-sensitized ZnO DSCs is higher than that of the D149-sensitized DSCs in the visible-wavelength (400–700 nm) region. It is important to recognize that the influence of thickness on the photocurrent of DSCs utilizing secondary ZnO nanoparticles is relatively small in comparison with utilizing tetrapod-like ZnO nanoparticles in our previous

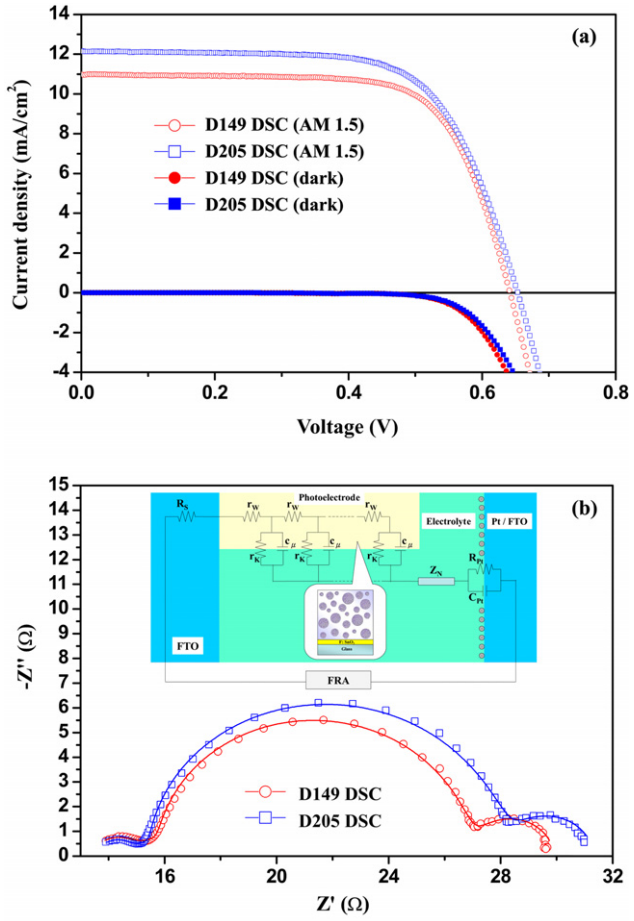

Figure 5. Photovoltaic characteristics of DSCs with 27 μm-thick ZnO photoelectrodes and two different indoline dyes. (a) J–V curves for D149- and D205-sensitized DSCs with AM 1.5 illumination and in the dark, respectively. (b) Nyquist plots of D149- and D205-sensitized DSCs performed under illumination at the applied bias of V_{oc}. The solid lines are the fitting results from the equivalent circuit model of ZnO DSCs (see inset).

report [9]. The possible explanation for this could be ascribed to the sufficient light harvesting capability of these hierarchical ZnO architectures even with quite thin photoelectrodes.

Figure 5(a) shows the detailed comparison of photocurrent–voltage (J–V) characteristics for solar cells constructed using 27 μm-thick ZnO photoelectrode films and these two indoline dyes under AM 1.5 full sunlight illumination (100 mW cm^{-2}) and in the dark. For D205 uptake, the J–V plot reveals V_{oc} = 0.653 V, J_{sc} = 12.17 mA cm^{-2}, FF = 0.67, and η = 5.34%. For comparison, the J–V plot of D149 uptake reveals V_{oc} = 0.641 V, J_{sc} = 10.94 mA cm^{-2}, FF = 0.71, and η = 4.95%. The resultant improvement in J_{sc} responds to the correspondingly higher IPCE for the D205-sensitized ZnO DSCs as compared with the D149-sensitized ZnO ones. The curves of dark current also indicate that D205-sensitized ZnO DSCs have a slightly more negative onset potential for the reduction of I_3^- than D149-sensitized ZnO DSCs. The lower dark current could also be rationalized in terms of a negative shift in the conduction band edge of ZnO caused by the adsorption of D205 dye. Both V_{oc} and J_{sc} for D205-sensitized ZnO DSCs are higher than D149-sensitized ones. The superior performance for D205 dye uptake can be ascribed to the effective suppression of electron recombination between I_3^- and efficient electron injection into the photoelectrodes by extending the alkyl chain on the terminal rhodanine moiety from ethyl to octyl [34]. Principally, the dyes with the hydrophobic alkyl chains would not only form a blocking layer over the sensitizer dye layer to protect the dye layer against water ingression from the electrolyte but also rearrange the dye orientating more perpendicular to the ZnO surface. The effects of different dyes on the electron transport of the interfaces in the DSCs can be further investigated with the aid of electrochemical impedance spectroscopy (EIS). Adequate physical models and equivalent circuits have been proposed and widely applied to analyze the electron transport in the photoelectrode and recombination between the photoelectrode and the electrolyte interface in DSCs [35–40]. The Nyquist plots of the impedance data for D149- and D205-sensitized ZnO DSCs were performed by applying a 10 mV ac signal over the frequency range of 10^2–10^5 Hz under illumination at the applied bias of V_{oc}. The Nyquist plots in figure 5(b) show that the radius of the middle semicircle, which belongs to D205-sensitized ZnO DSCs, is larger than that of D149-sensitized ZnO DSCs, indicating that the electron recombination resistance is enlarged from D149 to D205. Some interior parameters of the devices can be further derived by the good fitting of the impedance data of the Nyquist plots to the expressions based on the equivalent circuit of DSCs as shown in the inset of figure 5(b). $r_w = (R_w/L_F)$ is the transport resistance of the electrons in the ZnO electrode; $r_k = (R_k L_F)$ is the charge transfer resistance of the charge recombination between electrons in the ZnO electrode and I_3^- in the electrolyte. The thickness L_F of all anodes are about 27 μm; $C\mu = (c_\mu L_F)$ is the chemical capacitance of the ZnO electrode; R_s is a series resistance for the transport resistance of FTO and all resistances out of the cell; Z_N is the impedance of diffusion of I_3^- in the electrolyte; R_{Pt} and C_{Pt} are the charge transfer resistance and the interfacial capacitance at the counter electrode (platinized FTO glass)/electrolyte interface, respectively; R_{FTO} and C_{FTO} are the charge transfer resistance and the interfacial capacitance at the exposed FTO/electrolyte interface, respectively; R_{FZ} and C_{FZ} are the resistance and the capacitance at the FTO/ZnO contact, respectively. The fitted results are also listed in table 2 and include the first-order reaction rate for the loss of electrons (k_{eff}), the electron lifetime ($\tau = 1/k_{eff}$), the electron transport resistance (R_w), and the charge transfer resistance related to recombination of electrons at the ZnO/electrolyte interface (R_k). The electron-loss rate k_{eff} in the D205-sensitized ZnO DSCs is smaller than the D149-sensitized ones, which causes the prolonged electron lifetime in the D205-sensitized ZnO DSCs. The increase in electron lifetime supports more effective suppression of the back reaction of the injected electrons with the I_3^- in the electrolyte. This evidence can also be confirmed with the larger R_k value for D205-sensitized ZnO DSCs that indicates less interfacial recombination occurring between the ZnO and electrolyte interface. Moreover, the effective electron diffusion coefficient ($D_{eff} = (R_k/R_w)L_F^2 k_{eff}$) is also enhanced with utilization of the D205 sensitizer. In general, the current

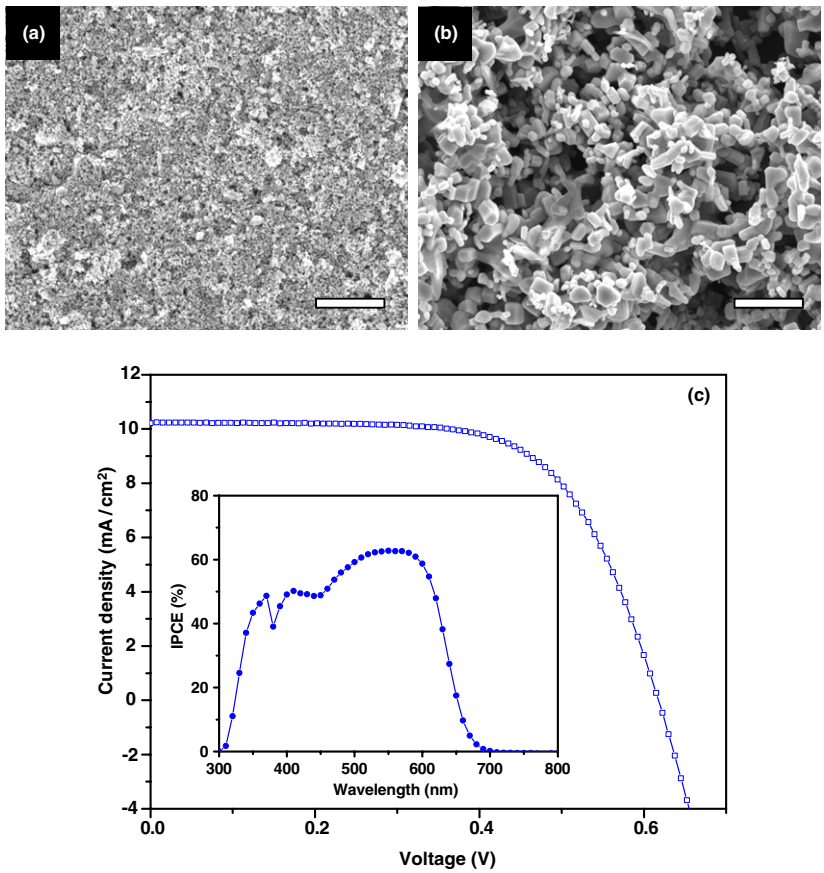

Figure 6. (a) FESEM image of non-aggregated primary ZnO nanocrystallites (size 8–10 nm) from grinding the original ZnO secondary nanoparticles; scale bar, 1 μm. (b) Commercial ZnO particles (Merck Ltd; broad size distribution, 100–600 nm) as a scattering layer on the top; scale bar, 1 μm. (c) J–V curve and IPCE spectrum (inset) of D205-sensitized DSCs composed of 23 μm-thick ground nanoparticles and 4 μm-thick commercial ZnO particles as a scattering layer on the top.

Table 2. Performances and electron transport properties of the D149- and D205-sensitized DSCs (27 μm-thick ZnO photoelectrode) determined by J–V characteristics and EIS analysis.

ZnO DSCs	J_{sc} (mA cm^{-2})	V_{oc} (V)	FF	η (%)	k_{eff} (s^{-1})	τ_{eff} (ms)	R_k (Ω)	R_w (Ω)	D_{eff} ($\times 10^{-3}$ cm^2 s^{-1})
D149	10.94	0.641	0.71	4.95	57.85	17.29	12.55	2.47	2.14
D205	12.17	0.653	0.67	5.34	47.12	21.22	14.43	1.98	2.51

density for DSCs is determined by the initial number of photogenerated carriers, the electron injection efficiency from dye molecules to semiconductor, and the recombination rate between the injected electrons and oxidized dye or redox species in the electrolyte. Based on the assumption of the same injection efficiency and dye loading for the given ZnO DSCs systems, it is reasonable that the photocurrent density may be directly affected by the variation in the electron recombination rate. The amphiphilic nature of D205 may assist the formation of a self-assembled dye monolayer that prevents the recapture of the photoinjected electrons by the triiodide ions within the electrolyte, consequently resulting in a higher V_{oc} and J_{sc} [5].

The compared ZnO DSCs composed of only primary nanocrystallites without any aggregation were also demonstrated as a contrast. Figure 6 shows the cell behaviors of D205-sensitized DSCs composed of 23 μm-thick primary nanoparticles (via girding the secondary ZnO nanoparticles) with 4 μm-thick commercial ZnO particles (Merck Ltd) as a scattering layer on the top. For the ground particles, the J–V curve reveals $V_{oc} = 618$ mV, $J_{sc} = 10.22$ mA cm^{-2}, FF $= 0.66$, and $\eta = 4.16\%$, for which the performance is poorer than the hierarchical ZnO photoelectrode. The IPCE spectrum also shows remarkable deterioration in the visible-wavelength (400–700 nm) region for the D205-sensitized DSC composed of ground nanoparticles because of insufficient light-traveling distance. The insufficient light harvesting for non-aggregated ZnO photoelectrodes also leads to increasing the non-excited area, which lowers V_{oc} further after averaging the electron density. From Cao's report [24, 25] the optical absorption spectra of the ZnO films consisting of aggregates will be affected by different sizes and size distributions. Normally, the scattering efficiency will shift to long wavelength when the secondary particle size is increasing. However, Cao *et al* specially indicate that polydisperse aggregates with a large average size

or broad size distribution could result in an obvious enhancement in the optical absorption and light harvesting efficiency of photoelectrode films due to Mie scattering. Moreover, the photoelectrode composed of broad size distributed secondary ZnO particles will be superior for obtaining compact films from screen-printing processes.

Comparative experiments reported on metal-free indoline dyes emphasize the importance of improving the photovoltaic performance by suitable molecular engineering. The unambiguous enhancement of photopower-conversion efficiency was examined by extending the length of the alkyl chain on the indoline sensitizer with a hierarchical photoelectrode composed of aggregated ZnO secondary nanoparticles. Although the efficiency of ZnO DSCs cannot compete with TiO_2 systems presently, we hope that these investigations will shed light on the development of organic sensitizers and can be used in the ZnO nanostructure optimization for the proposed solar cell applications.

4. Conclusion

In summary, D149 and D205 indoline dyes were used as the effective sensitizers for DSCs composed of hierarchical ZnO photoelectrodes. The higher charge transfer rate and retarded fluorescence decay reveal that D205 has better electron injection dynamics for ZnO nanoparticles as compared to D149. The optimal energy conversion efficiencies of 4.95% and 5.34% were achieved for D149 and D205 on 27 μm-thick ZnO photoelectrode films under AM 1.5 solar radiation. The significantly enhanced performance for D205-sensitized ZnO DSCs is ascribed to the effective suppression of electron recombination as well as enhancment of the interfacial electron transfer rate by extending the alkyl chain on the terminal rhodanine moiety. The results of the comparison of the electron transport property were further confirmed, presenting a prolonged electron lifetime in the D205-sensitized ZnO DSCs. Thus, the hybrid system of hierarchical ZnO architecture and metal-free indoline sensitizer may represent an alternative candidate for high-performance DSCs.

Acknowledgments

The authors acknowledge MCL/ITRI and PVTC/ITRI for facilities. This work was sponsored by MCL/ITRI through project No. 8301XSY4X1 and National Science Council (NSC) of Taiwan through grants No. NSC-96-2628-M-009-001-MY3 and NSC-96-2628-E-009-018-MY3.

References

[1] Grätzel M 2005 *Inorg. Chem.* **44** 6841–51
[2] Nazeeruddin M K, DeAngelis F, Fantacci S, Selloni A, Viscardi G, Liska P, Ito S, Takeru B and Grätzel M 2005 *J. Am. Chem. Soc.* **127** 16835–47
[3] Ito S *et al* 2006 *Adv. Mater.* **18** 1202–5
[4] Ito S, Miura H, Uchida S, Takata M, Sumioka K, Liska P, Comte P, Péchy P and Grätzel M 2008 *Chem. Commun.* 5194–6
[5] Kuang D, Uchida S, Humphry-Baker R, Zakeeruddin S M and Grätzel M 2008 *Angew. Chem. Int. Edn* **47** 1923–7
[6] Horiuchi T, Miura H and Uchida S 2003 *Chem. Commun.* 3036–7
[7] Horiuchi T, Miura H, Sumioka K and Uchida S 2004 *J. Am. Chem. Soc.* **126** 12218–9
[8] Oskam G, Hu Z S, Penn R L, Pesika N and Searson P C 2002 *Phys. Rev.* E **66** 011403
[9] Özgür Ü, Alivov Y I, Liu C, Teke A, Reshchikov M A, Doğan S, Avrutin V, Cho S J and Morkoç H 2005 *J. Appl. Phys.* **98** 041301
[10] Pearton S J, Norton D P, Ip K, Heo Y W and Steiner T 2005 *Prog. Mater. Sci.* **50** 293–340
[11] Law M, Greene L E, Johnson J C, Saykally R and Yang P 2005 *Nat. Mater.* **4** 455–9
[12] Baxter J B and Aydil E S 2005 *Appl. Phys. Lett.* **86** 053114
[13] Pasquier A D, Chen H and Lu Y 2006 *Appl. Phys. Lett.* **89** 253513
[14] Cheng H M, Chiu W H, Lee C H, Tsai S Y and Hsieh W F 2008 *J. Phys. Chem.* C **112** 16359–64
[15] Gonzalez-Valls I and Lira-Cantu M 2009 *Energy Environ. Sci.* **2** 19–34
[16] Martinson A B F, Elam J W, Hupp J T and Pellin M J 2007 *Nano Lett.* **7** 2183–7
[17] Martinson A B F, Góes M S, Fabregat-Santiago F, Bisquert J, Pellin M J and Hupp J T 2009 *J. Phys. Chem.* A **113** 4015–21
[18] Jiang C Y, Sun X W, Lo G Q, Kwong D L and Wang J X 2007 *Appl. Phys. Lett.* **90** 263501
[19] Hosono E, Fujihara S, Honma I and Zhou H 2005 *Adv. Mater.* **17** 2091–4
[20] Hosono E, Mitsui Y and Zhou H 2008 *Dalton Trans.* **40** 5439–41
[21] Hsu Y F, Xi Y Y, Yip C T, Djurišić A B and Chan W C 2008 *J. Appl. Phys.* **103** 083114
[22] Chiu W H, Lee C H, Cheng H M, Lin H F, Liao S C, Wu J M and Hsieh W F 2009 *Energy Environ. Sci.* **2** 694–8
[23] Chen W, Zhang H, Hsing I M and Yang S 2009 *Electrochem. Commun.* **11** 1057–60
[24] Zhang Q F, Chou T P, Russo B, Jenekhe S A and Cao G Z 2008 *Adv. Funct. Mater.* **18** 1654–60
[25] Zhang Q, Chou T P, Russo B, Jenekhe S A and Cao G 2008 *Angew. Chem. Int. Edn* **47** 2402–6
[26] Cheng H M, Hsu H C, Chen S L, Wu W T, Kao C C, Lin L J and Hsieh W F 2005 *J. Cryst. Growth* **277** 192–9
[27] Cheng H M, Lin K F, Hsu H C, Lin C J, Lin L J and Hsieh W F 2005 *J. Phys. Chem.* B **109** 18385–90
[28] Seelig E W, Tang B, Yamilov A, Cao H and Chang R P H 2003 *Mater. Chem. Phys.* **80** 257–63
[29] Cao H, Zhao Y G, Ho S T, Seelig E W, Wang Q H and Chang R P H 1999 *Phys. Rev. Lett.* **82** 2278–81
[30] Xu J, Zhang H, Liang G J, Wang L X, Xu W L, Gui W G and Li Z C 2010 *J. Serb. Chem. Soc.* **75** 259–69
[31] Ham H W and Kim Y S 2010 *Thin Solid Films* **518** 6558–63
[32] Jose R, Kumar A, Thavasi V and Ramakrishna S 2008 *Nanotechnology* **19** 424004
[33] Dentani T, Kubota Y, Funabiki K, Jin J, Yoshida T, Minoura H, Miura H and Matsui M 2009 *New J. Chem.* **33** 93–101
[34] Kroeze J E, Hirata N, Koops S, Nazeeruddin M K, Schmidt-Mende L, Grätzel M and Durrant J R 2006 *J. Am. Chem. Soc.* **128** 16376–83
[35] Bisquert J 2002 *J. Phys. Chem.* B **106** 325–33
[36] Bisquert J 2003 *Phys. Chem. Chem. Phys.* **5** 5360–4
[37] Bisquert J, Zaban A, Greenshtein M and Mora-Seró I 2004 *J. Am. Chem. Soc.* **126** 13550–9
[38] Wang Q, Moser J E and Grätzel M 2005 *J. Phys. Chem.* B **109** 14945–53
[39] Wang Q, Ito S, Grätzel M, Fabregat-Santiago F, Mora-Seró I, Bisquert J, Bessho T and Imai H 2006 *J. Phys. Chem.* B **110** 25210–21
[40] Adachi M, Sakamoto M, Jiu J, Ogata Y and Isoda S 2006 *J. Phys. Chem.* B **110** 13872–80